ELSEVIER

Biochimica et Biophysica Acta 1252 (1995) 312–320

BBA Biochimica et Biophysica Acta

Conformation of polymyxin B analogs in DMSO from NMR spectra and molecular modeling

Shih-Yi Liao, Geok-Toh Ong, Kung-Tsung Wang, Shih-Hsiung Wu *

Institute of Biological Chemistry, Academia Sinica and Institute of Biochemical Sciences, National Taiwan University, P.O. Box 23-106, Taipei, Taiwan

Received 1 August 1994; accepted 9 June 1995

Abstract

The tertiary structures of two polymyxin analogues:

and

in DMSO, from solid-phase peptide synthesis and aerobic oxidation were determined from two-dimensional NMR spectra and distance geometry calculations followed by restrained molecular dynamics simulation. The backbone of peptide **I** had a rectangular shape stabilized by at least two hydrogen bonds and the hydrophilic side chains of five lysine residues, and the hydrophobic side chains of Phe and Leu resided at both sides to form an amphiphilic molecule. This amphiphilic structure of **I** is likely to interact with lipid A mainly via a hydrophobic interaction. Compared with **I**, peptide **II**, which lacks three N-terminal amino-acid residues, exhibits neither amphiphilic property nor binding ability with lipid A.

Keywords: Polymyxin analogue; Peptide conformation; ROESY spectrum; Distance-geometry calculation; Restraint molecular dynamics simulation; NMR

1. Introduction

Polymyxins were first isolated from a strain of *Bacillus polymyxa* in 1947 [1,2]. Like most peptide antibiotics, they contain a mixture of D- and L-amino acids. The characteristics of polymyxin B (PMB) in terms of structure are a large fraction of 2,4-diaminobutanoic acid (Dab), a fatty acid attached to the peptide through an amide bond, and a heptapeptide ring that is formed by the amide bond between the γ-amino group of Dab in position 4 and the carboxyl group of the C-terminal [3]. PMB affects diverse biochemical processes in bacteria including selective membrane permeability [4], transport phenomena [5], respiration [5,6], and the synthesis of nucleic acids [5], proteins [5–8], lipopolysaccharides and peptidoglycans [5]. The primary effect arising from polymyxin B is believed to be binding to a bacterial membrane so as to alter its permeability [3,9,10]; all other effects on bacterial metabolism are likely secondary [3]. Another biological activity of polymyxin B is to detoxify lipopolysaccharide (LPS) and

Abbreviations: NMR, nuclear magnetic resonance; HPLC, high-performance liquid chromatography; DQF-COSY, double-quantum filtered correlation spectroscopy; HOHAHA, homonuclear Hartmann–Hahn spectroscopy; NOESY, nuclear Overhauser spectroscopy; ROESY, rotating frame nuclear Overhauser and exchange spectroscopy; NOE, nuclear Overhauser effect; DG, distance geometry; RMD, restrained molecular dynamics; RMSD, root mean square deviation; TFA, trifluoroacetic acid; DMSO, dimethylsulfoxide; HMP resin, *p*-hydroxymethylphenoxymethylpolystyrene resin; DAB, 2,4-diaminobutanoic acid; EDT, 1,2-ethandithiol; Fmoc-amino acid, *N*-fluorenylmethoxycarbonyl amino acid; LPS, lipopolysaccharide; PMB, polymyxin B.

* Corresponding author. Fax: +886 2 3635038.

SSDI 0167-4838(95)00127-1

prevent LPS-induced symptoms by binding with the lipid A of LPS. Because PMB contains a large fraction of D- and uncommon amino acids, PMB degrades slowly in a biological system and probably induces harmful side effects. For this reason polymyxins are seldom used in clinical treatment.

Attempts to explain the relationship between structure and function of PMB have been numerous [11–14]. The membrane activity of PMB is believed to correlate with its amphiphilic character. The structure of PMB includes a hydrophilic and polycationic heptapeptide ring moiety that may strongly interact with negatively charged phospholipid and LPS, and the hydrophobic acyl chain that might penetrate lipid membranes to form a PMB-lipid complex. Thus, the formation of the complex causes phase separation between PMB-bound lipid and free lipid in a cell membrane and results in a local lesion that alters the permeability. The cationic peptide polymyxin B nonapeptide (PMBN) is a part of the antibiotic polymyxin B that lacks the fatty acyl part of the parent compound [15]. PMBN is not bactericidal, but it can cause disorganization of the outer membrane of Gram-negative bacteria by binding to anionic groups of LPS [16,17].

Rustici et al. designed several polymyxin B analogs that were synthesized with lysine replacing Dab residues, L-Phe replacing D-Phe and cyclization via an intramolecular disulfide bridge as shown in Fig. 1 [18]. On biological testing, the decapeptide (**I**) revealed a large affinity to bind lipid A for detoxification, but almost no antibiotic activity was observed. Peptide **I**, which contains common L-amino acids, degrades readily in a biological system and shows no toxicity to animals. Therefore, with thermodynamic binding similar to that of a reaction between antigen and antibody, such a peptide **I** may provide a strategy for prophylaxis and treatment of LPS-mediated diseases. Peptide **II**, which comprises only the cyclic heptapeptide part of **I** without the three amino-acid residues at the N-terminus, shows no binding affinity to lipid A [18]. In order to compare the structures of peptide **I** and **II** and to study the relationship between structure and function, we chemically synthesized the two peptides, **I** and **II**, and investigated their tertiary structures in dimethylsulfoxide (DMSO) by means of NMR spectroscopy and molecular modeling.

2. Materials and methods

2.1. Preparation of peptides

The peptides resulted from solid-phase peptide synthesis. Starting with HMP resin (0.284 g, 0.25 mmol, 0.85 mmol/g), syntheses were conducted with an automated peptide synthesizer (ABI Model 431A). Fmoc-amino acids were introduced with the manufacturer's prepackaged cartridges (1 mmol each) with a stepwise protocol (*FastMoc*™). Side-chain protection was cysteine(Trt), lysine(Boc) and threonine(t-Bu); Trt, trityl; Boc, *t*-butyloxycarbonyl and t-Bu, *tert*-butyl. After synthesis, peptide resin (0.10 g) was placed in a spherical flask that contained a micro stir bar. The cool mixture containing EDT (0.15 ml), deionized H_2O (0.5 ml) and TFA (9.5 ml) was put into the flask. After stirring at 0°C for 30 min and subsequently at room temperature for 1.5 h, the reaction mixture was concentrated on a rotary evaporator; the temperature of the water bath was maintained below 40°C to prevent thermal damage to the peptide. Dichloromethane (10 ml) was added to help the solution evaporate. The crude reduced

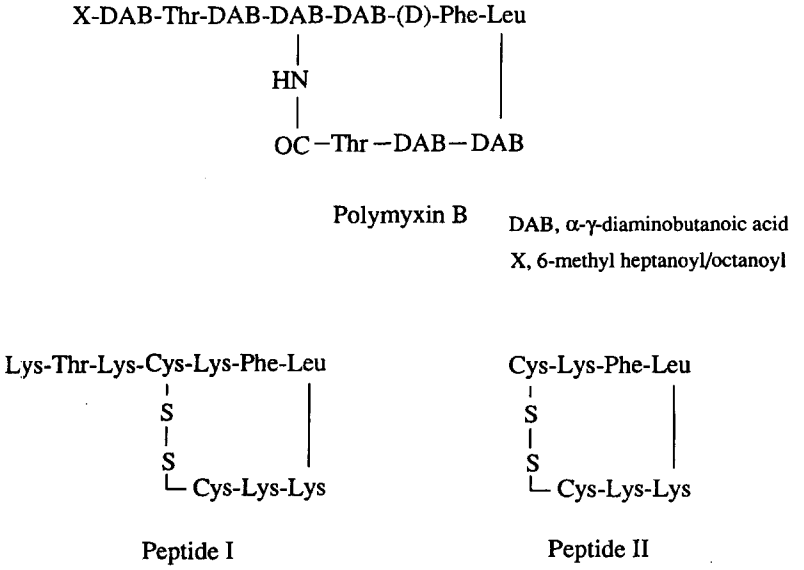

Fig. 1. Structures of polymyxin B and its analogues (peptides **I** and **II**). All amino acids have the L-configuration unless otherwise indicated.

peptide was triturated and washed with cold diethyl ether. After extraction with acetic acid (1%) solution and filtration to remove resin, the crude reduced peptide was immediately transferred to a stirred solution (1 l) of acetic acid (1%). After stirring for several minutes, the pH of the solution was adjusted to 8.0 with aqueous ammonium hydroxide. To form the intramolecular disulfide bond, the solution was maintained with stirring at 4°C for 120 h; the progress of oxidation in the peptide solution was measured by analytical HPLC at various intervals.

After oxidation, the crude peptide was obtained and further purified by HPLC on a semi-preparation column (Vydac C_{18}) applying a gradient (0/70/0% solvent B in 0/25/30 min; solvent A was H_2O/TFA = 100/0.1, and solvent B was acetonitrile/H_2O/TFA = 95/5/0.1) at a flow rate of 2 ml/min and UV monitoring at 214 nm. The purified peptides were characterized with a mass spectrometer (Jeol JMS-HX 110, fast atom bombardment) and amino-acid analysis (Beckman 6300 Amino Acid Analyzer).

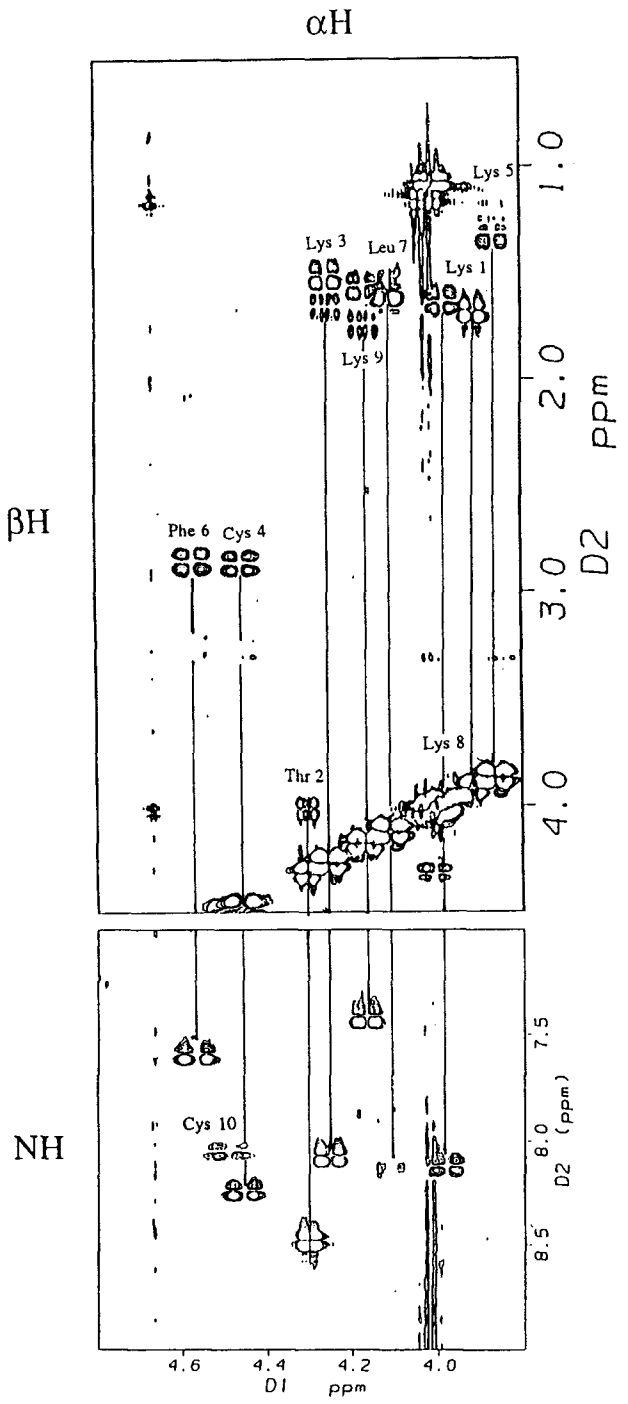

Fig. 2. Cross peaks of $C_\alpha H$–NH and $C_\alpha H$–$C_\beta H$ in the DQF-COSY spectrum of peptide **I** in DMSO-d_6 at 300 K.

2.2. NMR spectroscopy

The NMR samples (ca. 10 mg, 16 mM) were dissolved in DMSO-d_6 (0.5 ml). All NMR experiments were performed at 400 MHz (Bruker AM-400 or AMX-400 spectrometer). Chemical shifts are referred to the solvent signal at 2.49 ppm. Assignments of proton spectra of peptides **I** and **II** were made with techniques DQF-COSY [19,20], HOHAHA [21], NOESY [22] and ROESY [23]. Spectra were recorded in the phase-sensitive mode with time-proportional phase increment (TPPI) [22]. DQF-COSY and HOHAHA spectra were recorded at 300 K with 512 t_1 increments and 2048 complex points in the t_2 dimension. For ROESY and NOESY, 1024 data points were acquired in the t_2 dimension with 512 t_1 increments, respectively. In the HOHAHA experiments we applied a MLEV-17 spin-lock pulse sequence with mixing times of 70 and 120 ms. Mixing times of 60, 150 and 300 ms were used for NOESY and ROESY experiments. After zero filling to a 1K × 1K (for ROESY and NOESY) matrix or 2K × 2K (for DQF-COSY and HOHAHA) matrix, $\pi/2$-shifted squared sine-bell functions were applied in both dimensions prior to Fourier transformation. ROESY and NOESY spectra were processed on an IRIS workstation (Silicon Graphics, USA) using Felix software (version 2.10, Hare Research). The temperature coefficient of **I** and **II** were determined over a temperature range 27–57°C at 5°C interval. H–D exchange in NH protons was tested on adding D_2O in small aliquots with a microsyringe directly to a known amount of the compound in DMSO-d_6 in the NMR tube.

2.3. Computer modeling

The interproton distance information was derived by integrating the volume of the ROESY spectra cross peak. The interproton distances were derived from the equation.

$$r_{ij} = r_{lm}(\sigma_{lm}/\sigma_{ij})^{1/6}$$

r_{lm} was set to 1.78 Å for geminal protons of Cys as a

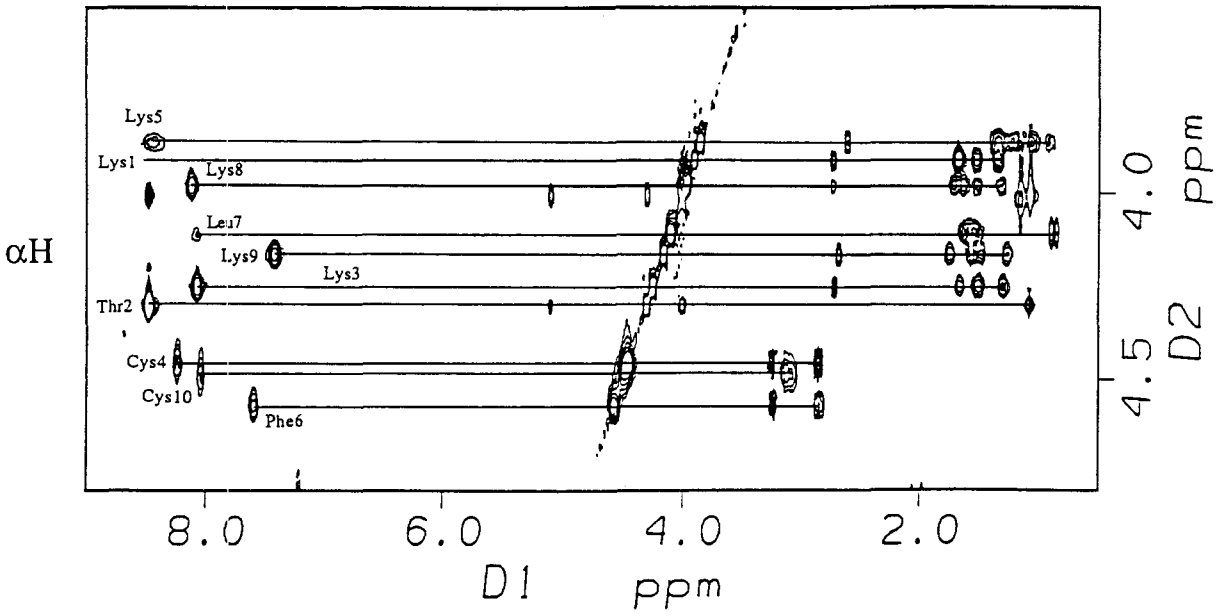

Fig. 3. Contour plot of the region of amide proton to side chain proton of peptide **I** in the HOHAHA spectrum (τ_m = 120 ms) that was used to assign amino-acid spin systems. Spin systems of all residues that contain amide protons, except K1, are shown. Horizontal lines connect the spin systems.

calibration distance. The ROESY cross-peak intensities were classified into three distance ranges, 1.8–2.8, 1.8–3.3 and 2.5–5 Å, corresponding to strong, medium and weak NOE, respectively, to compute the tertiary structure. All calculations were achieved on workstations (Silicon Graphics Iris 4D/35 and Indigo Elan 4000). Structures were analyzed with the macromodel computer-modeling system Insight II (version 2.2., Biosym). Structures were calculated in two protocols: one was the combined distance geometry-restrained molecular dynamics protocol (denoted DG-RMD) with DGII and Discover programs and a CVFF force field (Biosym, USA) to refine the tertiary structure, and the other involved only restrained molecular dynamics protocols. For both protocols ROE constraints were applied. Methyl and methylene protons without stereospecific assignments were treated as pseudoatoms, and pseudoatom corrections were added to the upper and lower distance constraints [24]. Thirty structures were obtained from the DGII calculation. One representative structure selected from DG structures and an extended structure with a disulfide bond were then used as starting structures for the second stage based on the restrained molecular dynamics. These RMD calculations proceeded in three stages; distance information was included using a skewed biharmonic potential that was equal for all restraints. In the first stage, 4.2 ps calculations consisting of 20 cycles were executed for heat and equilibrium at the temperature 300 or 1000 K. The NOE force constant gradually increased from 40 to 400 kJ/mol Å^2. This step was followed with another 10 ps RMD calculation with the same distance constraints for further equilibrium in the second stage with the force constant maintained at 400 kJ/mol Å^2. In the third stage, a further 20 ps RMD calculation was undertaken. The structures did not underwent in significant conformational alterations during the final 20 ps and were subjected to a further 200 cycles of conjugated gradient restrained energy minimization calculation.

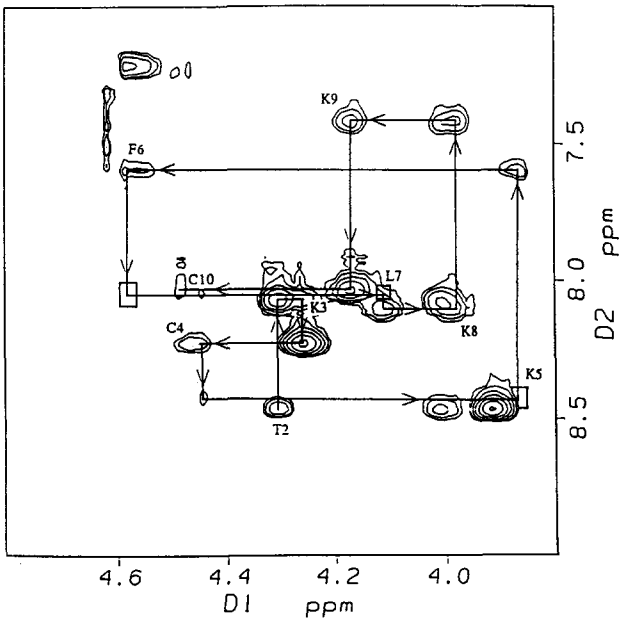

Fig. 4. Contour plot of the fingerprint region of peptide **I** in the ROESY spectrum recorded with mixing time 150 ms. Sequential $d_{\alpha N}$ connectivities are indicated by lines. Some COSY NH–C_αH cross peaks are labeled according to the sequential assignment.

3. Results and discussion

3.1. Synthesis of the polymyxin analog

Peptide **I** was prepared with a solid-phase peptide synthesizer and oxidized with air at 4°C. The linear, reduced peptide **I** had a retention time 15.74 min in HPLC analysis. After oxidation, a new feature corresponding to a retention time 16.58 min appeared on semi-preparative HPLC analysis that was confirmed to be due to the cyclic peptide by amino-acid analysis and mass spectrometry, m/z $(M+H)^+$: 1224.7. The progress of oxidation was clearly monitored with the decreased signal due to the linear, reduced peptide and the increased signal due to the cyclic oxidized peptide for durations of oxidation 1, 8, 24 and 120 h.

The synthesis of peptide **II** was similar to that of **I**. Further evidence of correct molecular weight appeared in the mass spectrum from the feature at m/z $(M+H)^+$: 867.7.

3.2. Assignment of chemical shifts

Sequence-specific assignments of NMR signals of peptide **I** were made according to the conventional method developed by Wüthrich [25]. First, the NMR signals in DQF-COSY and HOHAHA spectra were assigned to spin systems of specific amino-acid types. Fig. 2 displays a representative region of the DQF-COSY spectrum. All expected cross peaks between amide and $C_\alpha H$ proton were observed except Lys-1 and Lys-5. The correlations of chemical shifts between amide and $C_\alpha H$ protons were extended to side-chain protons by means of the HOHAHA spectrum (Fig. 3); the chemical shifts of Lys-1 and Lys-5 were readily identified according to this spectrum. The second step was to align the sequence of spin systems based on the primary structure of **I** by ROESY experiments that were done to establish connectivities through space between neighboring amino-acid residue protons. The cyclic decapeptide (**I**) contained a disulfide bond to

Table 1
^1H Chemical shifts of peptide **I** in DMSO-d_6 at 300 K

Residue	Chemical shift/ppm of			
	N-H	α-H	β-H	Others
Lys-1		3.92	1.70	γCH$_2$ 1.38, 1.38 δCH$_2$ 1.53, 1.53 εCH$_2$ 2.75, 2.75 εNH$_2$ 7.80
Thr-2	8.47	4.30	4.00	γCH$_3$ 1.09
Lys-3	8.06	4.27	1.51, 1.67	γCH$_2$ 1.30, 1.30 δCH$_2$ 1.50, 1.50 εCH$_2$ 2.73, 2.73 εNH$_2$ 7.80
Cys-4	8.24	4.45	2.87, 3.28	
Lys-5	8.42	3.88	1.21, 1.39	γCH$_2$ 0.92, 0.92 δCH$_2$ 1.08, 1.08 εCH$_2$ 2.62, 2.62 εNH$_2$ 7.80
Phe-6	7.60	4.58	2.86, 3.24	2,6H 7.22
Leu-7	8.10	4.12	1.54, 1.54	γH 1.65; δCH$_3$ 0.85, 0.91
Lys-8	8.12	3.98	1.64, 1.72	γCH$_2$ 1.32, 1.32 δCH$_2$ 1.51, 1.51 εCH$_2$ 2.75, 2.75 εNH$_2$ 7.80
Lys-9	7.42	4.17	1.57, 1.75	γCH$_2$ 1.28, 1.28 δCH$_2$ 1.50, 1.50 εCH$_2$ 2.70, 2.70 εNH$_2$ 7.80
Cys-10	8.04	4.49	3.09, 3.14	

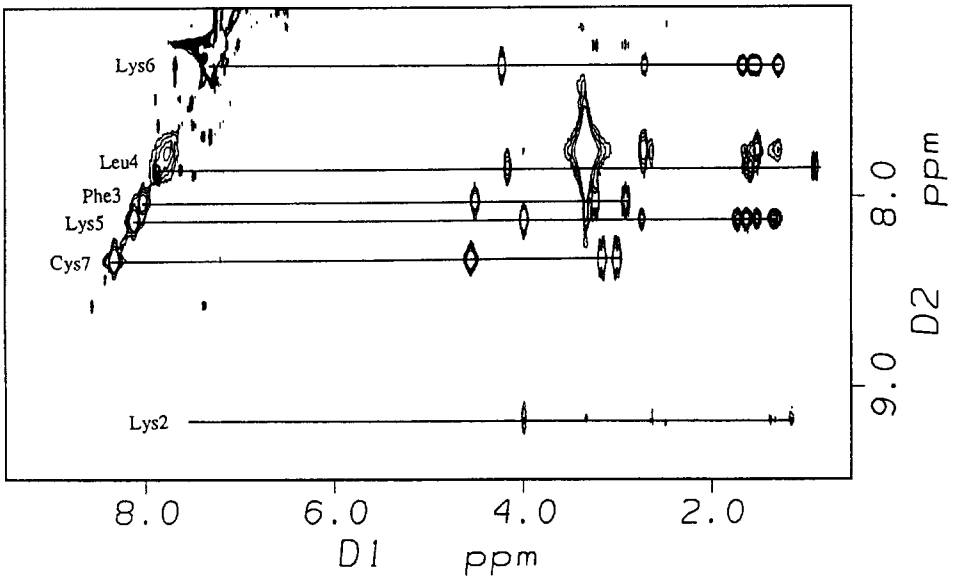

Fig. 5. HOHAHA spectrum of peptide **II** recorded with 120 ms mixing time. Spin systems of all residues, except C_1, are shown. Horizontal lines connect the spin systems.

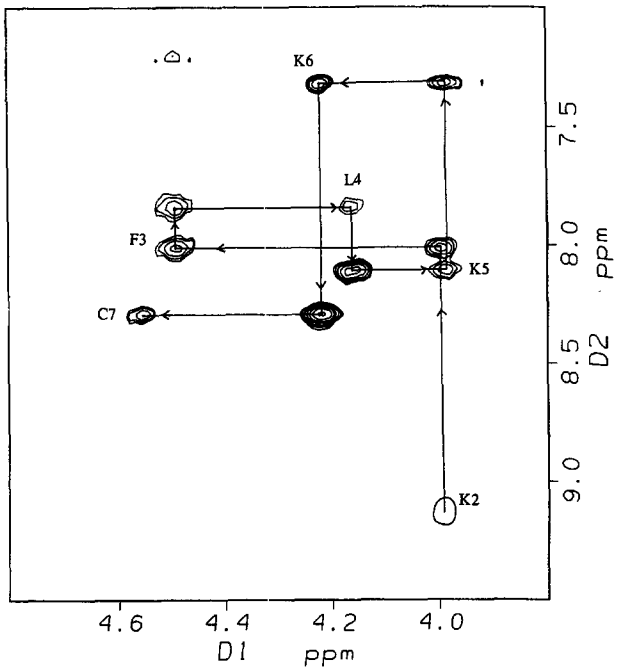

Fig. 6. Fingerprint region of peptide **II** in DMSO-d_6 in the ROESY spectrum recorded at 300 K with a mixing time 300 ms. Sequential $d_{\alpha N}$ connectivities are indicated for the sequence of residues 2–7. Some COSY NH–CαH cross peaks are labeled according to the sequential assignment.

Table 2
^{1}H chemical shifts of peptide **II** in DMSO-d_6 at 300K

Residue	Chemical shift/ppm of			
	N-H	α-H	β-H	Others
Lys-2	9.18	4.00	1.36	γCH_2 0.98, 0.98 δCH_2 1.14, 1.14 εCH_2 2.62, 2.62 εNH_2 7.79
Phe-3	8.02	4.51	2.91, 3.22	2,6H 7.11
Leu-4	7.85	4.16	1.59, 1.59	γH 1.62; δCH_3 0.89, 0.92
Lys-5	8.11	3.98	1.64, 1.72	γCH_2 1.33, 1.33 δCH_2 1.51, 1.51 εCH_2 2.74, 2.74 εNH_2 7.79
Lys-6	7.31	4.22	1.55, 1.57	γCH_2 1.28, 1.28 δCH_2 1.52, 1.52 εCH_2 2.71, 2.71 εNH_2 7.77
Cys-7	8.33	4.54	3.00, 3.17	

form a closed ring and five lysine residues in positions 1, 3, 5, 8 and 9 were clearly identified. All assignments were completed through sequential connectivities shown in Fig. 4. The chemical shifts of all protons in **I** are summarized in Table 1.

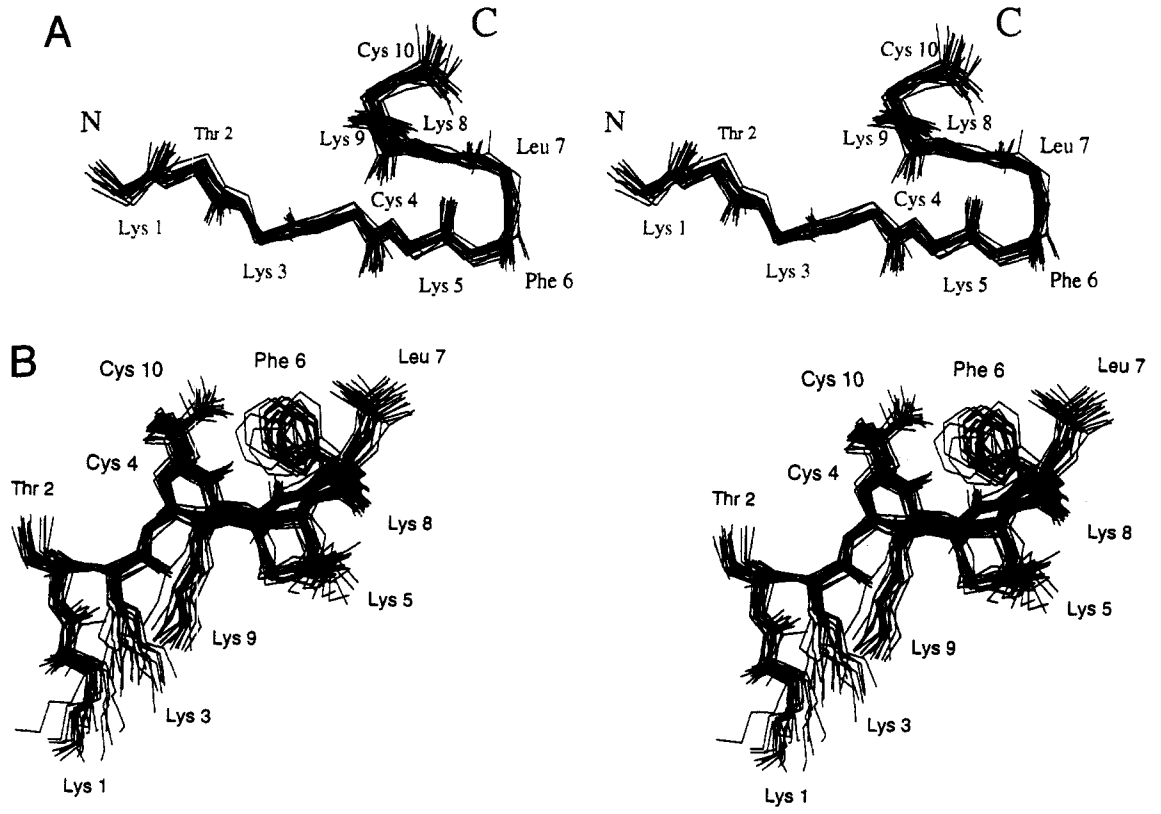

Fig. 7. Stereo view of twenty selected RMD structures of peptide **I**. The superposition was the best fit of backbone atoms (N, Cα, C′ and O) shown in (a) and heavy atoms shown in (b).

Table 3
Dihedral angle/deg for a representative structure of both peptides.

Peptide **I**					Peptide **II**				
	ϕ	ψ	ω	C-S-S-C		ϕ	ψ	ω	C-S-S-C
Lys-1	–	131	177		Cys-1	–	120	−170	
Thr-2	−115	89	−161		Lys-2	−169	87	−144	
Lys-3	−158	107	−166		Phe-3	−81	140	173	
Cys-4	−86	139	−179		Leu-4	−151	−68	158	
Lys-5	−130	155	−179		Lys-5	−152	66	−177	
Phe-6	−88	94	5		Lys-6	−133	−73	166	
Leu-7	−130	102	−172		Cys-7	−98	–	–	103
Lys-8	177	111	−174						
Lys-9	83	140	−156						
Cys-10	33	–	–	−82					

Table 4
Distance/10^{-10} m of hydrogen bonds and disulfide bridge for a representative structure of both peptides.

Peptide	Hydrogen bonds		-S-S-
	$NH_{(5)}$–$CO_{(8)}$	$NH_{(8)}$–$CO_{(5)}$	
I	2.28	2.34	2.00
II	–	–	2.07

The same method was applied to assign NMR spectra of peptide **II**. The HOHAHA and ROESY recordings for sequential connectivities in Figs. 5 and 6, respectively. Chemical shifts of all protons except Cys-1 in **II** are summarized in Table 2. The missing signal of Cys-1 in NMR spectra was also observed in the case of ω-conotoxin GVIA [26].

3.3. Collection of constraints from NMR parameters

According to certain assumptions, NOE is related to the distance between interacting nuclei and this information from NMR spectra is the most important to determine the tertiary structure of proteins and peptides. Because the correlation time of molecules of moderate size such as

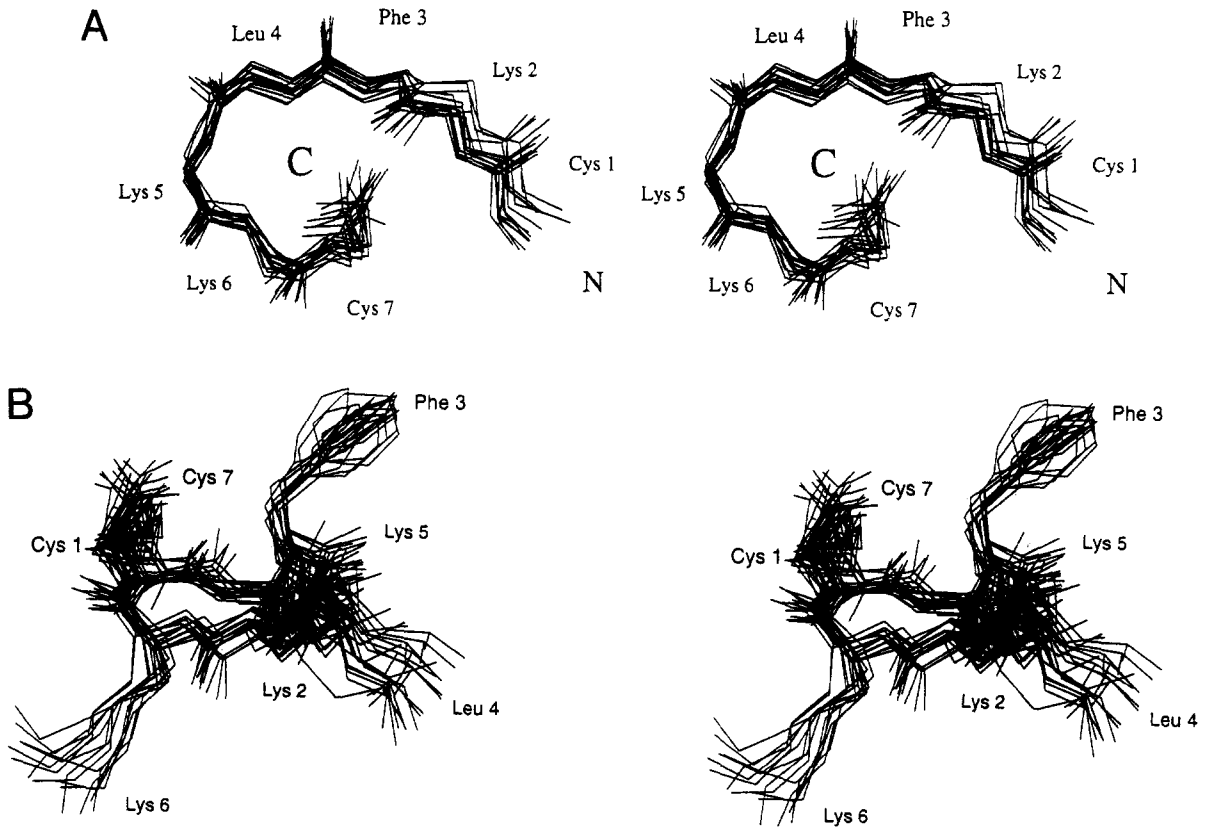

Fig. 8. Stereo view of twenty selected RMD structures of peptide **II**. The superposition was the best fit of backbone atoms (N, Cα, C′ and O) shown in (a) and heavy atoms shown in (b).

Table 5
Temperature dependence of the amide N-H proton chemical shift of peptide **I** [a] as $(\Delta\delta_{NH}/\Delta T)$/ppb/K.

	Thr-2	Lys-3	Cys-4	Lys-5	Phe-6	Leu-7	Lys-8	Lys-9	Cys-10
$\Delta\delta_{NH}/\Delta T$	3.83	2.07	4.47	2.62	1.88	3.47	3.83	1.44	4.46

[a] $\Delta\delta_{NH}/\Delta T$ of all residues of peptide **II** is large.

peptides **I** and **II** makes the rate of cross relaxation nearly zero, only a few cross peaks were found in NOESY spectra. ROESY spectra recorded at varied mixing times provided better results [27,28]. The H_β cross peak of Cys was chosen as the reference standard with a distance 1.78 Å. Subsequently, cross peaks with varied contour levels or intensity in ROESY spectra with mixing time 150 ms were rationalized to their corresponding distances. The ROE constraints of pseudoatoms without stereospecific assignments are explicitly taken into consideration as Wüthrich et al. described [24]. Thus, in the case of **I**, 74 distance constraints, 60 intraresidual and 14 interresidual, were derived from the ROESY cross peaks. However, in the case of **II**, only 32 intraresidual and sequential constraints were collected, and no constraints of medium and long distance were found.

Additional conformational constraints were obtained from analysis of the vicinal protons (NH-CαH) that indicated a dependence on the torsional angle [29]. The coupling parameters ($^3J_{HN\alpha}$) of amide protons of Cys-4, Lys-5, Phe-6, Leu-7, Lys-8 and Lys-9 extracted from 1D-^{1}H spectra are in the range 8–9 Hz, which correspond to the range of torsional angle [−180, −80].

3.4. Calculation of distance geometry and molecular modeling

The initial structure for distance geometry calculation was constructed with the computer modeling program Insight II. 30 structures with similar conformation were generated from DG calculation and were clustered into a single family with RMSD values less than 1.0 Å for backbone atoms. Based on the least-energy and least-ROE constraint violations, a representative structure was chosen as initial structure to calculate the restrained molecular dynamics.

The selected DG structure was subsequently optimized and refined according to the RMD method, to obtain energetically stable structures with minimum violations of distances and dihedral angles. For **I**, 20 structures were selected from 355 total simulated RMD structures; they were superimposed for the best fit of backbone atoms (N, Cα and C′) and heavy atoms shown in Fig. 7. The average RMSD values from the mean structure are 0.473 Å for backbone atoms and 0.677 Å for heavy atoms.

In the case of **II**, 15 selected structures were superimposed for the best fit of backbone atoms (N, Cα and C′) and heavy atoms shown in Fig. 8. The average RMSD values from the mean structure are 0.528 Å for backbone atoms and 0.981 Å for heavy atoms. The dihedral angles, hydrogen bonds distances and disulfide bridge geometry for a representative structure of both peptides are listed in Tables 3 and 4.

In order to assess the accuracy of RMD protocol, two initial structures, a linear structure with a disulfide bond constraint and a DG structure with 1000 steps of conjugate potential minimization, were used for the RMD calculation. Similar results obtained from these two initial structures confirmed the accuracy of the RMD protocol.

3.5. Character of tertiary structure and relation to its function

Shown in Fig. 7a, the backbone of peptide **I** exhibited a bent rectangular shape, and hydrophilic side chains of five

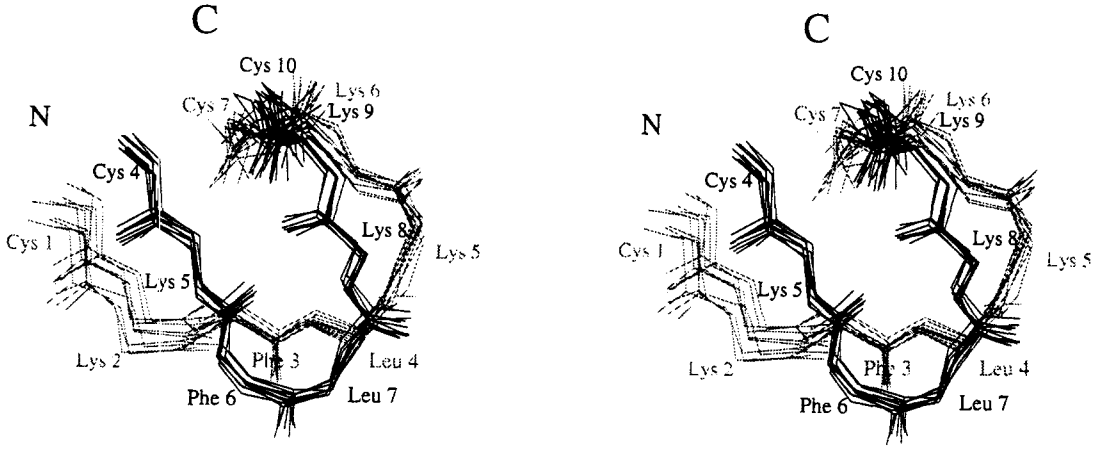

Fig. 9. Best-fit superposition of backbone atoms of peptide **I** [4–10] fragment (dark lines) and peptide **II** (light lines). These two peptides have ten selected RMD structures.

Lys residues (1, 3, 5, 8 and 9) and hydrophobic side chains of Phe-6 and Leu-7 reside at both sides to form an amphiphilic molecule. According to structural analysis of **I**, the backbone of the bent rectangular shape is stabilized by two hydrogen bonds, $NH_{(5)}$–$CO_{(8)}$ (or $NH_{(5)}$–$CO_{(9)}$) and $NH_{(8)}$–$CO_{(5)}$. These two hydrogen bonds are confirmed by experiments on H–D exchange and temperature dependence of the amide N–H proton chemical shifts (Table 5). Two long-range ROE, Lys-1 H_{β}/Lys-9 H_{δ} and Cys-4 H_{α}/Cys-10 NH, are the main forces that keep positive charges of the side chain of 5 Lys at one side and make the molecule amphiphilic. The backbone structure of **II** has a doughnut pattern. Because of lack of long- and medium-range ROE, no hydrogen bonds were found in the ring closure. Unlike the structure of **I**, the side chains of Phe-3 and Leu-4 in **II** are dispersed at the two sides of the ring closure. Consequently, peptide **II** loses an amphiphilic property and reveals no binding affinity with lipid A. The peptide **II** and the heptapeptide ring moiety (4–10 residues) of peptide **I** are superimposed in Fig. 9 and show distinct shapes that result from the addition of three amino-acid residues at the N-terminus of **I**. According to a previous report, the binding of **I** to lipid A was unaffected by pH or ionic strength [18]; thus the hydrophobic binding probably involves the side chains of Phe-Leu which is in the cyclic, conformationally stable peptide structure. The designed peptide (**I**) that contains five L-Lys residues with its structure defined from NMR spectra and molecular modeling reveals an amphiphilic property. However, unlike natural cationic and amphiphilic peptides such as melittins, which have strong hemolytic activity on red blood cells, peptide **I** has no lytic activity on human erythrocytes [18].

The detailed mechanisms of the interaction between polymyxin B and bacterial outer membranes at the molecular level are still poorly understood. Elucidation of the binding site at lipid A according to peptide structures may enhance our understanding of the nature of mammalian receptor proteins for LPS. Therefore, a peptide drug that possesses great activity and slight toxicity might be designed for treatment of prophylaxis and LPS-mediated diseases.

Acknowledgements

We thank Mr. Fong-Ku Shi for measuring NMR spectra in M & Vactek Corporation Taiwan, and Dr. Li-Chin Chuang and Mr. Chyh-Chong Chuang for critically reading the manuscript.

References

[1] Ainsworth, G.C., Brown, A.M. and Brownlee, G. (1947) Nature 160, 263.
[2] Benedict, R.G. and Langlykke, A.F. (1947) J. Bacteriol. 54, 24–25.
[3] Storm, D.R., Rosenthal, K.S. and Swanson, P.E. (1977) Annu. Rev. Biochem. 46, 723–763.
[4] Rosenthal, K.S., Swanson, P.E. and Storm, D.R. (1976) Biochemistry 15, 573–576.
[5] Teuber, M. (1974) Arch. Microbiol. 100, 131–144.
[6] Pruul, H. and Reynolds, B.L. (1972) Infect. Immunol. 6, 709–717.
[7] Ennis, H.L. (1965) J. Bacteriol. 90, 1102–1108.
[8] Ennis, H.L. (1965) J. Bacteriol. 90, 1109–1119.
[9] Vaara, M. and Vaara, T. (1983) Antimicrob. Agents Chemother. 24, 114–122.
[10] Schindler, P.R.G. and Teuber, M. (1975) Antimicrob. Agents Chemother. 8, 95–104.
[11] Schröder, G., Brandenburg, K. and Seydel, U. (1992) Biochemistry 31, 631–638.
[12] Hartmann, W., Galla, H.-J. and Sackmann, E. (1978) Biochim. Biophys. Acta 510, 124–139.
[13] Chapman, T.M. and Golden, M.R. (1972) Biochem. Biophys. Res. Commun. 46, 2040–2047.
[14] Galardy, R.E., Craig, L.C. and Printz, M.P. (1974) Biochemistry 13, 1674–1677.
[15] Chihara, S., Tobita, T., Yahata, M., Ito, A. and Koyama, Y. (1973) Agric. Biol. Chem. 37, 2455–2463.
[16] Vaara, M. and Vaara, T. (1983) Nature, 303, 526–528.
[17] Kubesch, P., Boggs, J., Luciano, L., Maass, G. and Tümmler, B. (1987) Biochemistry 26, 2139–2149.
[18] Rustici, A., Velucchi, M., Faggioni, R.; Sironi, M., Ghezzi, P., Quataert, S., Green, B. and Porro, M. (1993) Science 259, 361–365.
[19] Marion, D. and Wüthrich, K. (1983) Biochem. Biophys. Res. Commun. 113, 967–974.
[20] Rance, M., Sørensen, O.W., Bodenhausen, G., Wagner, G., Ernst, R.R. and Wüthrich, K. (1983) Biochem. Biophys. Res. Commun. 117, 479–485.
[21] Bax, A. and Davies D.G. (1985) J. Magn. Reson. 65, 355–360.
[22] Bodenhausen, G., Kogler, H. and Ernst, R.R. (1984) J. Magn. Reson. 58, 370–388.
[23] Kessler, H., Griesinger, C., Kerssebaum, R., Wagner, K. and Ernst, R.R. (1987) J. Am. Chem. Soc. 109, 607–609.
[24] Wüthrich, K., Billeter, M. and Braun, W. (1983) J. Mol. Biol. 169, 949–961.
[25] Wüthrich, K. (1986) NMR of Protein and Nucleic Acids, Wiley, New York, NY.
[26] Skalicky, J., Metzler, W.J., Ciesla, D.J., Galdes, A. and Pardi, A. (1993) Protein Sci. 2, 1591–1603.
[27] Kessler, H., Gehrke, M. and Griesinger, C. (1988) Angew. Chem. Int. Ed. Engl. 27, 490–536.
[28] Davis, D.G. and Bax, A. (1985) J. Magn. Reson. 70, 207–213.
[29] Karplus, M. (1963) J. Am. Chem. Soc. 85, 2870–2871.